JOURNAL OF CATALYSIS 145, 464–478 (1994)

Chromia Supported on Titania

III. Structure and Spectroscopic Properties

U. Scharf,* H. Schneider,† A. Baiker,† and A. Wokaun*,[1]

*Physical Chemistry II, University of Bayreuth, D-95440 Bayreuth, Germany; and †Department of Chemical Engineering and Industrial Chemistry, Eidgenössische Technische Hochschule Zürich, CH-8092 Zürich, Switzerland

Received March 19, 1993; revised August 11, 1993

The surface structure and the oxidation state of chromia catalysts supported on titania are investigated by vibrational spectroscopy, UV–visible diffuse reflectance measurements, and X-ray photoelectron spectroscopy (XPS). Pronounced changes are observed as the chromia loading is varied between 0.5 and 30 wt%. While isolated surface-bound chromate ions prevail at low coverages, an increasing fraction of trimeric and tetrameric clusters, as well as of higher aggregates, is observed for chromia contents ≥10 wt%. On the 0.5% CrO_x/TiO_2 catalyst, chromia species in a formal oxidation state of V represent the most abundant surface species, with a significant contribution of Cr (VI). As the chromia coverage is increased, the fraction of Cr(V) is found to decrease, while a growing contribution from Cr(III)/Cr(IV) species is detected. *In situ* calcination studies show that the temperature of conversion of the $Cr(NO_3)_3$ precursor (deposited by incipient wetness impregnation) into the oxidized surface chromate species depends on coverage. With 3 wt% chromia content, coordinatively unsaturated surface chromyl species are observed to develop around 373 K, whereas for 30 wt% chromia coverage, conversion into coordinatively saturated surface chromyl species takes place around 413 K. Laser Raman experiments show that the surface chromia supported on titania does not undergo laser-induced crystallisation under the conditions used.

INTRODUCTION

In view of their favourable catalytic properties, supported chromium oxide systems are extensively applied in technical catalytic processes (1, 2). Bulk chromia is active for the selective catalytic reduction (SCR) of NO with ammonia, but also catalyzes the direct oxidation of ammonia at higher temperatures (3). The latter is a problem which may be avoided by the use of amorphous chromia catalysts (4). In studies of supported chromia systems, silica (5a) or alumina have been mostly used as carrier materials. An investigation of CrO_x/ZrO_2 was reported by Cimino *et al.* (5b), while chromia supported on titania has received comparatively little attention (6). In a project aimed at the development and characterization of CrO_x/TiO_2 catalysts for SCR, we have recently reported on EPR parameters (7) and catalytic performance (8) of these systems (Parts I and II of this study, respectively).

Several publications (1, 9) have focussed on a comparison between different supports. It has been established (10) that the SCR activity depends on the surface chromia species, and is largely uninfluenced by the bulk chromium oxide (Cr_2O_3) phase. A knowledge of the local surface structure, and of the factors by which it is determined, therefore plays an important role in understanding the catalytic properties, and in optimizing the catalyst systems. Several oxidation states were found to be present on the catalyst surfaces simultaneously (5, 9, 11). Hardcastle and Wachs (1) have characterized chromia/titania catalysts subsequent to calcination at high temperatures, i.e., at 773 and 973 K. Only Cr(VI) species were identified after calcination at 773 K, whereas a partial conversion to lower oxidation states was detected after calcination at 973 K.

In the present project, CrO_x/TiO_2 catalysts with chromia concentrations ranging from 0.5 to 30 wt% are investigated. Previous studies have concentrated on the EPR parameters of these systems both prior to and after calcination (7), as well as on catalytic properties in the selective catalytic reduction of nitric oxide (8). Here we are focussing on the surface state subsequent to calcination at 573 K; the simultaneous presence of at least three oxidation states of chromium is detected. Relative contributions are derived from XPS and UV–visible diffuse reflectance spectra.

Raman spectroscopy is used to obtain structural information on the supported chromia species. While Raman scattering has been established to provide detailed infor-

[1] To whom correspondence should be addressed.

0021-9517/94 $6.00

mation on clusters and agglomerates of supported chromium (VI) species, the characterisation of lower valence states is impeded by ligand field ($d \leftrightarrow d$) transitions in the visible spectral range, which give rise to a decrease in Raman intensity due to absorption and interference effects (12). As a consequence, studies in the literature have focussed either on unsupported Cr_2O_3 systems, in crystalline or amorphous modifications (4, 13–15), or else on supported catalysts with low chromia contents on titania (≤6 wt%) (1, 16). Recently, a Raman investigation of up to 30 wt% of chromia on Al_2O_3 (2) prepared by wet impregnation and an XPS study of ≤20 wt% of chromia on ZrO_2 (17) have been reported. In the present contribution, the prevailing chromia surface species are characterized over the full range from 0.5 to 30 wt% of chromia loading; the dependence on laser exposure and on calcination temperature is investigated by Raman and *in situ* FTIR spectroscopy.

EXPERIMENTAL

Catalyst Preparation

Impregnation of the titania carrier (70% anatase, 30% rutile; Degussa P25) was performed by the incipient wetness technique, using appropriate amounts of $Cr(NO_3)_3 \cdot 9\ H_2O$. Water was removed in a rotary evaporator during slow heating to 363 K over 10 h. Subsequently, the catalysts were calcined in oxygen at 573 K for 3 h. A detailed description of the preparation procedure has been given in Part I (7).

Unless explicitly stated otherwise, all measurements reported refer to this calcined state of the catalyst, which corresponds to *ex situ* calcination with respect to the spectroscopic measurements.

Spectroscopic Measurements

Diffuse reflectance IR spectra were recorded on two FTIR instruments. Characterisation of *ex situ* preconditioned samples was carried out on a Digilab instrument (Model FTS 80) equipped with an "environmental chamber" placed into a diffuse reflectance accessory (Spectra-Tech). A total of 512 scans have been accumulated for each spectrum, at a resolution of 2 cm^{-1}. The sample cell was purged with a small flow of oxygen during the measurements. *In situ* calcination studies performed using this instrument will be presented in Figs. 4 and 5. For this purpose, a batch of uncalcined catalyst was prepared by incipient wetness impregnation of TiO_2 with $Cr(NO_3)_3$ followed by drying. A small fraction was powdered, mixed with KBr, and heated *in situ* in the FTIR instrument under a continuous flow of dry oxygen. The temperature was raised to 473 K in steps over a period of 1 h. This somewhat milder treatment on a *powdered* specimen is intended to stimulate the bulk *ex situ* calcination procedure, in which a quantity of ≈10 g of *uncrushed* material is heated from room temperature to 573 K during 30 minutes.

Another set of *in situ* calcination studies, shown in Fig. 6, was performed on a Perkin–Elmer instrument (Model 1710) equipped with an environmental chamber (Starna, Model HCV-D3). Here an aliquot of the uncalcined catalyst powder was calcined *in situ* at 573 K for 1 h in a flow of 6% oxygen in argon (flow rate 100 ml/min). Thereafter, the sample was cooled to room temperature, and 200 scans were accumulated at 4 cm^{-1} resolution. For subsequent reduction, the sample was exposed to a flow (100 ml/min) of 6% hydrogen in argon at 573 K for 1 h, and spectra were recorded at room temperature as above.

Raman spectra were excited using either the 514.5 nm line of an argon ion laser (Spectra Physics, Model 2025-05) or the 531 nm line of a krypton ion laser (Coherent, model Innova 300). A 5–12 mW beam was focused onto a 0.15 mm diameter circular area on the sample. For detection, a triple spectrograph equipped with a cooled intensified diode array detector was used; this system has been described and characterised elsewhere (18).

Composite Raman bands were decomposed into Voigt profiles by means of a nonlinear least squares fitting procedure, implemented on a UNIX workstation. The width of the Gaussian component was fixed to correspond to the spectral resolution used, 5 cm^{-1}, as determined by the slit widths chosen. For each band, this Gaussian was convoluted with a Lorentzian profile of variable width, to be determined by the fit. As an input, the program was given starting values for the number of components, approximate frequency positions, and widths. If, however, the proposed number of lines exceeded that required for adequate fitting of the spectrum, the program would automatically eliminate the unnecessary band by shifting it outside the spectral range considered, or by excessive broadening.

X-ray photoelectron (XPS) spectra were recorded in a UHV apparatus (Leybold) equipped with a high pressure chamber ($p \leq 1$ MPa), a preparation chamber ($10^{-6} - 10^5$ Pa), and an analysis chamber ($\geq 10^{-8}$ Pa). The sample was positioned and transferred between the stages on a heatable/coolable sample rod. XPS measurements were performed at a base pressure of 2×10^{-7} Pa, using Mg $K\alpha$ primary radiation (13 kV, 10 mA). The pass energy of the 200 mm hemispherical analyzer was set at 200 eV. An energy step width of 200 meV, and a dwell time of 100 ms were chosen; 10 scans have been accumulated for each spectrum. A more detailed description of the apparatus has been given in Ref. (19).

UV–visible spectra were recorded on a spectrometer (Perkin–Elmer, Model Lambda 19) equipped with an integration sphere. The diffuse reflectance spectra were recorded under ambient conditions, using either $BaSO_4$ or

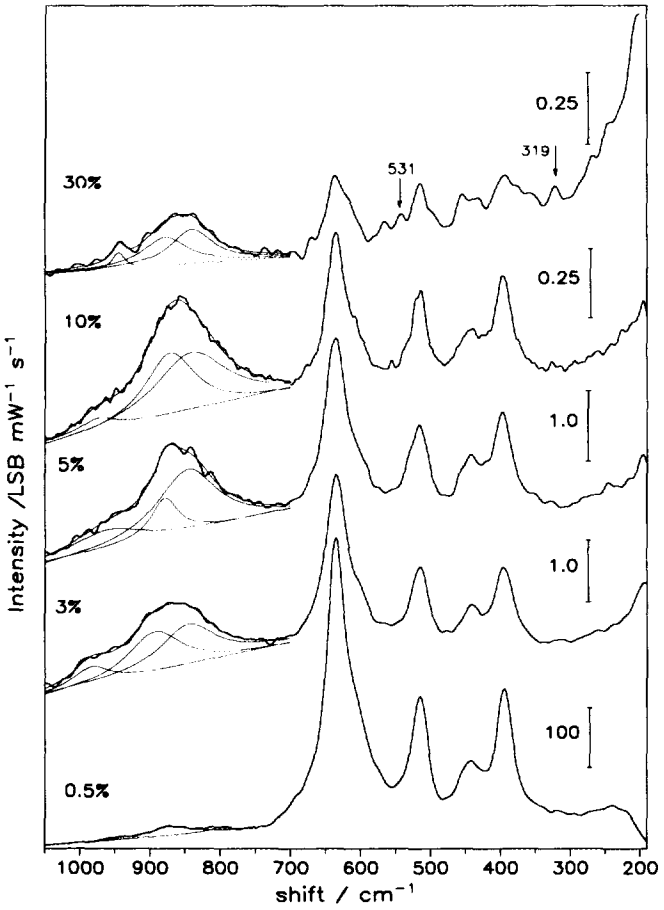

FIG. 1. Raman spectra of *ex situ*-calcined CrO_x/TiO_2 catalysts, excited at 514.5 nm using 5 mW of power. The chromia loading (in wt%) was varied as indicated in the figure.

KBr as a reference. For simulation, the spectra were first transformed to the Kubelka–Munk function. Subsequently the composite profile was represented as a superposition of Gaussian bands, the frequency positions and line widths being varied by the fit. Starting with a minimum number of components, the number of bands was increased until an adequate representation of the spectrum was achieved.

RESULTS

Raman Spectroscopy

Laser Raman spectra of the catalysts containing 0.5–30 wt% of Cr_2O_3 supported on TiO_2 are presented in Fig. 1. For chromia contents up to 10 wt%, the spectral region below 700 cm^{-1} is dominated by the well-known vibrations of the TiO_2 support (20, 21). In the 750–1000 cm^{-1} range, all catalysts exhibit vibrational bands originating from Cr(VI) species; Cr_2O_3 does not exhibit high frequency vibrations, but only gives rise to bands between 300 and 650 cm^{-1} (1). (For reference, the Raman spectra of unsupported commercial Cr_2O_3 and CrO_3 samples are shown later in Fig. 8.)

For the lowest loading, namely ≈0.5 wt% of chromia, a weak broad band is observed at ≈872 cm^{-1}; Hardcastle and Wachs (1) have assigned this vibration to an isolated tetrahedral surface species, which is distorted by interaction with the support. When the chromia content is increased to 3 wt%, the broad feature grows in intensity, and appears shifted to ≈870 cm−1. This composite band is decomposed into two peaks by the nonlinear least squares fitting procedure described in the Experimental section. The fit result is included in Fig. 1. Two bands at 845 cm^{-1} {ν_{as}(Cr–O–Cr)} and at 902 cm^{-1} {$\nu_s(CrO_3)$} are identified. The third, visibly separated band at 983 cm^{-1} is assigned to $\nu_s(CrO_2)$, according to Ref. (1). These three vibrations originate from nonterminal chromate units (22, 23). We note the drastic decrease in intensity of the support bands due to the covering of the surface by chromia, as may be seen by comparing the relevant intensity calibration bars.

The spectrum of the 5 wt% CrO_x/TiO_2 catalyst shows an increase in intensity of the feature at 870 cm^{-1}. Decomposition by the fit yields three vibrations centered at 845, 879, and 961 cm^{-1}. The pair of bands at 845 and at 961 cm^{-1} is indicative of trimeric and tetrameric chromium oxide chains, according to Hardcastle and Wachs (1).

For a loading of 10 wt% of chromia (fourth trace in Fig. 1), we again observe a maximum at 879 cm^{-1} due to isolated Cr(VI) species. In addition, band positions at 974 and 842 cm^{-1} were obtained from the nonlinear least squares fit, and are assigned to the stretching vibrations of tri- and tetrameric species (1, 2), as above.

At the highest loading (30 wt%), the pair of bands at 841 cm^{-1} {ν_{as}(Cr–O–Cr)} and at 945 cm^{-1} {$\nu_s(CrO_2)$ and $\nu_{as}(CrO_3)$ (1)} have become clearly resolved, showing that mainly tri- and tetrameric species are present on the surface of this catalyst sample. This statement is supported by indications of weak vibrational bands at 531 cm^{-1} {ν_s(Cr–O–Cr)} and 319 cm^{-1} {$\delta(CrO_3)$}, which are marked by arrows in the top trace of Fig. 1. In addition, a substantial fraction of isolated species is identified by the deconvolution procedure, from the band positioned at 878 cm^{-1}.

It is worthwhile to compare the intensities of the vibrational modes arising from the anatase fraction of the P25 support, over the series of catalysts investigated. The intensity decreases with increasing chromia content, as paralleled by a gradual color change from bright yellow (0.5 wt% Cr_2O_3) through brown and gray to dark black at higher loadings (≥10 wt%). For a chromia content of 30%, the loading exceeds that of a theoretical monolayer coverage (8.25 wt% as calculated for Cr_2O_3 (8)), and the support bands are correspondingly weak.

UV–Visible Spectroscopy

The observed changes in visible color of the catalysts suggest that different oxidation states and/or different coordination spheres of chromia are present on the respective surfaces. The use of UV–visible diffuse reflectance spectroscopy for monitoring such changes has been firmly established in the literature both for chromium (24) and for other transition metals (25–27). Diffuse reflectance spectra of our catalyst samples are presented in Fig. 2.

The spectra have been modelled as a superposition of Gaussian bands included as dashed lines in the figure, according to the procedure described in the Experimental part. The number of components was restricted to the minimum required for an adequate representation of the spectrum; the calculated envelope is included as a thin solid line in Fig. 2. In view of the intense coloration of the samples, and of the shape of the reflection spectra which show broad bands and comparatively little structure, not too much weight should be attributed to the precise frequency positions of the peaks. Even so, the decomposition into several bands is helpful for describing the changes occurring as a function of chromia loading, at least for the spectral range below 30,000 cm^{-1}.

The spectrum of the 0.5 wt% CrO_x/TiO_2 sample does not exhibit absorptions at energies below 21,000 cm^{-1}. We conclude that $d \leftrightarrow d$ excitations are not observed, which indicates an oxidation state of VI for the chromia centers. From a deconvolution of the absorption edge, charge transfer (CT) absorptions of tetrahedrally coordinated Cr(VI) centers are suggested, i.e., a forbidden $^1A_1 \rightarrow {}^1T_1$ transition at 22,600 cm^{-1}, and the first allowed $^1A_1 \rightarrow {}^1T_2$ transition at 29,800 cm^{-1}. The second allowed CT transition of Cr(VI), at 35,800 cm^{-1}, is concealed by the intense charge transfer absorptions of the titania support. The band positions for all the catalysts investigated are summarized in Table 1.

In the spectrum of the 2 wt% CrO_x/TiO_2 sample, a $d \leftrightarrow d$ transition appears at 14,500 cm^{-1}. In agreement with the work of Zecchina *et al.* (24), and with EPR results obtained on our catalyst samples (7), this transition energy is assigned to a Cr(V) species. The corresponding absorption increases in intensity and broadens for the 3 wt% chromia sample. Upon further increase of the chromia content up to 10 wt%, the $d \leftrightarrow d$ transition becomes very intense. The broadness of the feature suggests that additional oxidation states, such as Cr(III), may be present.

The center of the second band obtained from the deconvolution procedure shifts from 22,600 to 19,900 cm^{-1} as the chromia content is increased from 0.5 to 10 wt%. Unresolved absorptions due to Cr(III) are likely to be responsible for this apparent shift.

At a chromia loading of 30 wt%, the *calcined* catalyst sample appears visually black; results from diffuse reflectance spectroscopy must therefore be interpreted with care. A $d \leftrightarrow d$ transition centered at 13,200 cm^{-1} is identified from the fit. Together with the bands at 17,200 and 25,200 cm^{-1}, this absorption is assigned to a Cr(III) species in octahedral coordination (28). The additional presence of other oxidation states, such as Cr(V) and Cr(VI), is indicated, for example, by the transition observed at 20,600 cm^{-1}.

The *uncalcined* 30 wt% chromia catalyst, which appears green-blue to the eye (Fig. 2, bottom), exhibits a $d \leftrightarrow d$ transition at 17,300 cm^{-1} and a CT transition at 23,400 cm^{-1}, which are known from Cr(III) oxide (28). Differences between this result and those of more surface sensitive techniques will be addressed below.

Absorption bands at 16,400 cm^{-1}, which would be indicative of Cr(IV) (29), have not been identified with certainty on either of the catalyst samples.

X-Ray Photoelectron Spectroscopy

More detailed information on the oxidation states of chromium is obtained from XPS, which has been successfully applied to related catalyst systems (5, 17, 30, 31). The results recorded on our catalysts (0.5, 3, 10, and 30 wt% Cr_2O_3) are summarised in Table 2. To compensate for possible charging effects, binding energies have been normalized with respect to the position of the C 1*s* signal. The latter was held constant at 285.0 eV, i.e., the value chosen in Ref. (30).

The range of binding energies containing the Cr 2*p* and Ti 2*s* signals is presented in Fig. 3. The broad chromium $2p_{1/2}/2p_{3/2}$ doublets apparently represent a superposition of contributions from several oxidation states. For analysis, each composite peak shape was deconvoluted into three doublets with binding energies and spin–orbit splittings that are characteristic for Cr(VI) (E_B = 579.1–580.3 eV, ΔE = 9.1 eV (17,32)), Cr(V) (E_B = 577.5–578.5 eV, ΔE = 9.1–9.4 eV (9, 33)), and Cr(III) (E_B = 576.2–577.8 eV, ΔE = 9.8 eV (17,32)). The 2*p* binding energy of Cr(IV) is close to that of Cr(III); the multiplet splitting of Cr(IV) amounts to 9.7–9.8 eV (33), and the peak width is somewhat larger as compared to Cr(III) (5a). In view of these very similar parameters, no attempts have been made to separate a possible contribution of Cr(IV).

In the analysis, a Shirley background was used as a baseline. The deconvolution procedure becomes significant by the requirement that *both* the Cr $2p_{3/2}$ band position and the multiplet splitting must be consistent with the ranges that are characteristic for each species. As a test, the intensity ratio for the doublet components of a given species was not fixed during the fit; Table 2 shows

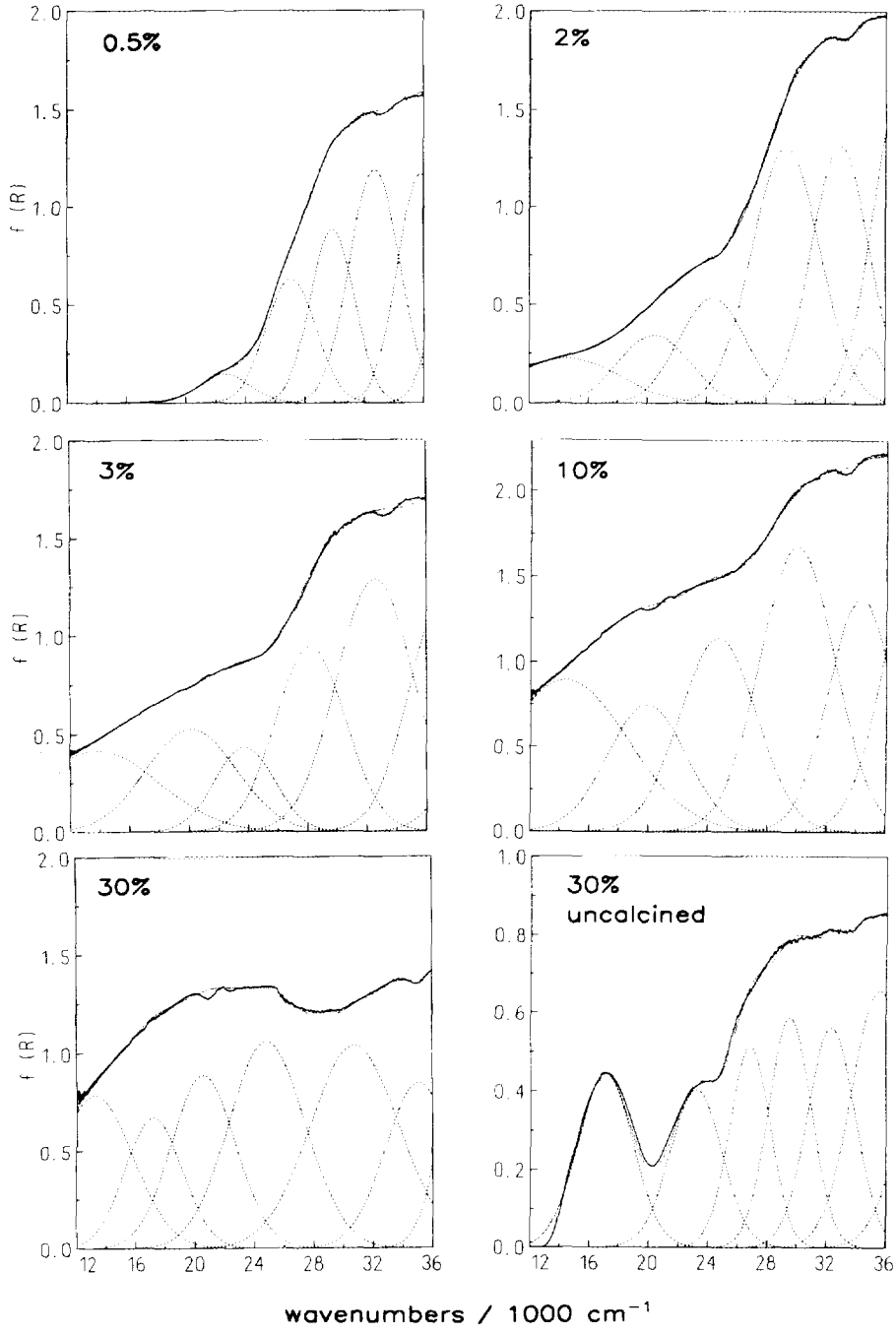

FIG. 2. UV–visible diffuse reflectance spectra of *ex situ*-calcined CrO_x/TiO_2 catalysts containing various chromia loadings. The bottom right spectrum was recorded on an *uncalcined* sample.

that the results obtained for this ratio varied between 0.50 and 0.49, i.e., very close to the theoretically expected value of 1 : 2.

It should be emphasized that with the restrictions indicated, an adequate fit of the spectra in terms of two oxidation states is not possible. In particular, the steep descent and the low energy tail of the $2p_{3/2}$ doublet component are well reproduced by the modelling only when a third oxidation state of low binding energy, i.e., Cr(III), is taken into account.

Peak positions, spin orbit splittings, and intensities obtained from the fit are listed in Table 2; the corresponding individual doublets and their calculated superposition are included in Fig. 3. The splitting and the binding energy

TABLE 1

UV–Visible Diffuse Reflectance Spectra of Titania-Supported Chromia Catalysts: Band Positions Obtained from Spectral Deconvolution

CrO_x content (wt%)	Spectral range ≤21,000 cm^{-1}				Spectral range ≥21,000 cm^{-1}[a]			
	Cr(III) (10^3 cm^{-1})	Cr(V) (10^3 cm^{-1})	Cr(III) (10^3 cm^{-1})	Cr(VI) + Cr(III) (10^3 cm^{-1})	Cr(VI) $^1A_1 \rightarrow {}^1T_1$ (10^3 cm^{-1})	(10^3 cm^{-1})	Cr(VI) $^1A_1 \rightarrow {}^1T_2$ (10^3 cm^{-1})	Cr(VI) (10^3 cm^{-1})
0.5					22.6		29.8	35.8
2		14.5		20.4		24.4	29.3	35.0
3		14.0		20.4		23.7	28.4	
10		14.4		19.9		24.7	30.0	
30	13.2		17.2	20.6		25.2	31.4	35.7
30 uncalcined			17.3			23.4	29.6	35.6

[a] The range of the Cr(VI) charge transfer bands overlaps with that of intense absorptions of the TiO_2 support.

obtained for Cr(VI) are close to the values expected from theory (9). For all oxidation states, the binding energies (Table 2) are consistently found to be at the low side of the intervals given in the literature, as specified above. We attribute these low binding energies to an influence of the titania support. The higher splitting of the Cr(V) doublet, as compared to that reported for Cr^{5+} on Al_2O_3 (9, 33), may also be due to a weaker interaction with the support.

Without the use of an X-ray monochromator, instrumental resolution is better than eV. With the additional constraint derived from the multiplet splitting, the differences in binding energies between the three oxidation states separated in Table 2 are therefore clearly significant. We reemphasize that any signal due to Cr(IV) would coincide with the Cr(III) peak. The fact that the peak positions determined for the Cr(III) doublet are close to the lower edge of the interval given for this oxidation state in the literature (17, 32) might be taken as an indication for the presence of Cr(IV). Some evidence for an involvement of Cr(IV) has also been obtained from an analysis of the reflection spectra of CrO_2 reference samples, as will be described elsewhere. Previous EPR studies (7) have shown Cr(IV) to be present after reduction with hydrogen or ammonia. After *ex situ* calcination, which corresponds to the state of most samples investigated in this study, the oxidation states +6, +5, and +3 were found to prevail (7, 8).

TABLE 2

Parameters Obtained from Deconvolution of XPS Spectra

Cr concentration (wt%)	Band position: Cr $2p_{1/2}$ (eV)	Band position: Cr $2p_{3/2}$ (eV)	Multiplet splitting ΔE (eV)	Intensity ratio $I(1/2)/I(3/2)$	Oxidation state	Intensity (10^3 counts s^{-1})	Intensity (%)	Binding energy Ti 2*s* (eV)	Intensity (10^4 counts s^{-1})
0.5	588.3	579.3	9.0	0.50	6+	1.9	25	565.9	2.92
	587.0	577.5	9.5	0.50	5+	4.9	66		
	585.2	575.3	9.8	0.50	3+	0.68	9		
3	588.6	579.4	9.2	0.50	6+	7.1	29	565.3	2.39
	587.1	577.5	9.6	0.50	5+	12.9	52		
	586.0	576.3	9.7	0.49	3+	4.7	19		
10	588.5	579.4	9.1	0.49	6+	12.1	34	565.7	2.34
	587.1	577.6	9.5	0.49	5+	15.2	43		
	586.0	576.1	9.8	0.49	3+	8.2	23		
30	588.3	579.1	9.2	0.49	6+	10.3	31	565.9	1.07
	587.7	577.7	9.4	0.49	5+	12.5	37		
	586.0	576.2	9.8	0.49	3+	10.5	32		
30 uncalcined	587.8	578.2	9.6	0.48	5+	14.0	100	565.9	1.05
30 uncalcined, sputtered	586.2	576.4	9.8	0.48	3+	21.4	100	565.6	0.70

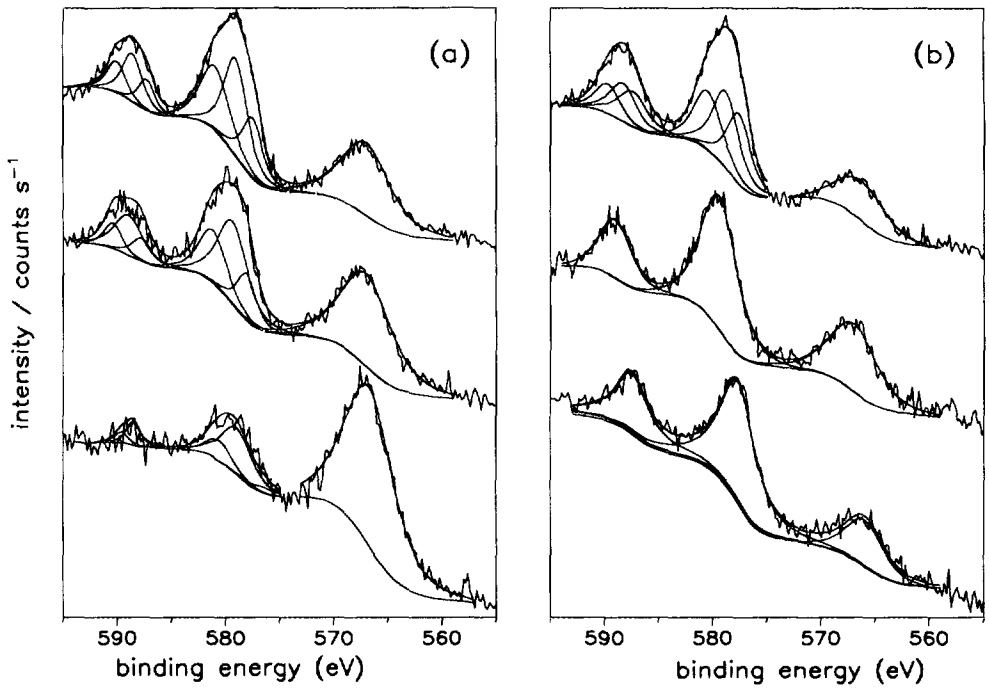

FIG. 3. XPS spectra of CrO_x/TiO_2 catalysts, recorded as described in the Experimental section. The spectral region containing the Cr 2*p* and Ti 2*s* signals is presented. Diagram (a), bottom to top, and top trace of diagram (b) correspond to *ex situ* calcined samples with chromia contents of 0.5, 3, 10, and 30 wt%, respectively. The middle spectrum in (b) was recorded on an *uncalcined* sample containing 30 wt% of chromia. The bottom spectrum in (b) was registered after the same sample had been sputtered with argon ions (sample current 5.5 μA, area 2 × 2 mm^2, sputter time 400 s).

The relative contributions of the three oxidation states, as determined from the fitting procedure, are now discussed in sequence for the investigated catalysts, and compared with the results from other spectroscopies. On all catalysts, a large fraction of Cr(V) is found, together with smaller contributions of Cr(VI) and Cr(III) on each catalyst. The percentage of Cr(V) decreases with increasing amount of chromia immobilized on the surface. The Cr(VI) fraction exhibits a moderate increase from 25 to 31% of the detected chromium. The most significant change is found for the relative contribution of Cr(III), which increases from 9% at 0.5 wt% CrO_x, up to 32% for the highest chromia loading of 30 wt%. For the latter catalyst, approximately equal amounts of the three oxidation states are coexisting on the spectroscopically accessible surface.

The intensity of the Ti 2*s* peak at 565.7 eV decreases for chromia loadings of 10 and 30 wt%, as expected from the increasing covering of the surface by chromia species. The fact that the Ti 2*s* signal remains detectable even above a monolayer coverage of chromia, is in agreement with the Raman spectra described above.

For the *uncalcined* sample containing 30 wt% of chromia, the best fit to the spectrum is obtained in terms of a single doublet at 578.2 eV with a splitting of 9.6 eV, which is characteristic of Cr(V). We recall that the catalyst was prepared by the incipient wetness method from $Cr(NO_3)_3$ solution. The prevalence of Cr(V) appears to be a consequence of oxidation of the outermost $Cr(NO_3)_3$ layers by atmospheric oxygen. This is demonstrated by a sputtering experiment: after a sputtering time of 400 s, the spectrum shown in the bottom trace of Fig. 3b is observed. In the fit, this spectrum is best represented by a single doublet, with a binding energy of 576.4 eV and a splitting of 9.8 eV. These parameter values are characteristic for Cr^{3+} (32). The presence of NO_3^- on this surface is confirmed by the observation of a nitrogen 1*s* peak at 407.8 eV in the XPS spectrum (not shown). The high binding energy (34) may be a consequence of the interaction of the nitrate ions with chromia centers or with the support. We note that the N 1*s* signal is absent on the calcined catalyst, as nitrate is lost during the calcination procedure.

To access the validity of these results, it is important to discuss the possible interference of any reduction caused by the sputtering process. Okamoto *et al.* (33) have found photoreduction to occur only after ≥30 min of sputtering time, on a very similar system. Our sputtering interval amounts only to 400 s, so that we may assert that the observed changes in oxidation state are real. A further

test was performed to support this statement: for a fully oxidized sample, *no* change in the oxidation state was seen even after ≥700 s of sputtering time.

It is interesting to compare our results from the XPS sputtering experiment with the characterization by diffuse reflectance spectroscopy, where a predominance of absorption peaks due to Cr^{3+} had been found (see above). We attribute this difference to the higher penetration depth of the visible light; note that a coverage as high as 30 wt% corresponds to a massive layer of chromia on the titania support. With the uncalcined sample stored under ambient conditions, the surface sensitive X-ray photoelectron spectroscopy detects the presence of a surface layer consisting of Cr(V). Upon sputtering, the unoxidized core consisting of Cr(III) is uncovered, which represents the majority of the material, and is therefore probed by UV spectroscopy. This remark also applies to the EPR results where all spins present in the sample are detected, and where a predominance of Cr^{3+} was found for the uncalcined sample.

In situ FTIR Study of the Calcination Process

Structural changes occurring at the catalyst surface during calcination have been monitored for the sample containing 30 wt% of Cr_2O_3. Subsequent to incipient wetness impregnation of the TiO_2 with $Cr(NO_3)_3$ and drying, a small fraction, powdered and mixed with KBr, was heated to 473 K *in situ* in the FTIR instrument under a continuous flow of dry oxygen, in steps of 50 K over a period of 1 h. This treatment is intended to simulate the bulk calcination procedure, in which a quantity of ≈10 g of uncrushed material is heated from room temperature to 573 K during 30 min.

In the range of chromyl stretching vibrations (850–1100 cm^{-1}), a broad feature is observed at room temperature (bottom trace in Fig. 4b); the observed band shape suggests a superposition of at least three bands. A vibration at 1048 cm^{-1} in this range has been assigned to the symmetric stretching vibration of nitrate ions (35); absorptions at 1033 and 1016 cm^{-1} are attributed by several authors to a monooxo chromyl species with a tetrahedral coordination (6, 10, 14, 36). When the temperature is raised to 373 K, the intensity of the absorption due to NO_3^- decreases. As a consequence, the principal maximum is observed at 1025 cm^{-1}, and represents a superposition of vibrations at 1033 and 1016 cm^{-1}.

At a temperature of 413 K, two new absorptions appear at 967 and 946 cm^{-1} indicating the formation of tetrameric chromate species; the assignment of the various chromate species is derived from investigations on chromium (VI) oxo salts by Mattes (37). The transformation of chromium nitrate into chromates is completed after the sample is held at 413 K for half an hour (fourth trace in Fig. 4b). The spectrum is now dominated by a broad band with a maximum at 947 cm^{-1} and a shoulder at 967 cm^{-1}. Between 1000 and 1050 cm^{-1} only weak and unstructured absorptions are detected.

Raising the temperature to 423 K gives rise to a modest sharpening of the band at 947 cm^{-1} ($\nu_s(CrO_2)$ and $\nu_{as}(CrO_3)$ (1)). There are indications of two weak shouldes at 904 and 880 cm^{-1} (both due to $\nu_s(CrO_3)$ (1, 37)). At 473 K these shoulders have developed into separate peaks. This pattern of three bands matches the one observed for $K_2Cr_4O_{13}$ (37). We note that these vibrations may also be compared with those observed on the surface of bulk chromia, where a variety of chromia species corresponding to different surface oxidation states has been described (15). The frequencies observed at 473 K correspond to coordinatively saturated surface chromyl species in a formal oxidation state of VI, which are distinguished by ligand heterogeneity in the bridging surface ligands (species III and VI in Ref. (15)).

An *in situ* FTIR study of the calcination for a sample with a lower chromia content (3 wt%) is presented in Fig. 4a. We note that the spectrum resulting after calcination is different from the one shown above in Fig. 4b. The $\nu(NO_3^-)$ vibration at 1047 cm^{-1} in the spectrum of the uncalcined sample is relatively weak, and overlapping with several other bands of comparable intensity in the same spectral region. Bands at 1015 and 998 cm^{-1} have been assigned to chromium ions with one vacant coordination site, while the absorption at 1025 cm^{-1} corresponds to a twofold coordinatively unsaturated species on α-Cr_2O_3 and on amorphous chromia (15). The absorption below 990 cm^{-1} originates from the $\nu(Cr{=}O)$ stretching vibrations of several coordinatively saturated chromia species on the surface of the titania support.

Temperature-induced processes become observable at 373 K; this temperature is lower by ≈40 K as compared to the 30 wt% catalyst. During calcination, an intense peak at 1018 cm^{-1}, and a broader band extending from 960 to 890 cm^{-1} are observed to grow. This pattern has been assigned to an oxidation state of chromia close to V (5, 6). If we again draw the analogy with species of the same formal oxidation state observed on bulk chromia, the vibration at 960–890 cm^{-1} could be ascribed to centers characterised by three oxygen ligands in bridging position to the bulk or the underlying support, one coordinative vacancy, one chromyl group with a bond order near two, and one further ligand (oxygen or hydroxyl) in bridging position to another chromia surface center. (For these species, which were designated as V and IX in a previous paper (15), IR bands at 1015, 995, and 980 cm^{-1} have been reported.) Further heating to 473 K does not result in new spectral features. The final spectrum is significantly different from that of the catalyst containing 30 wt% chromia, where a

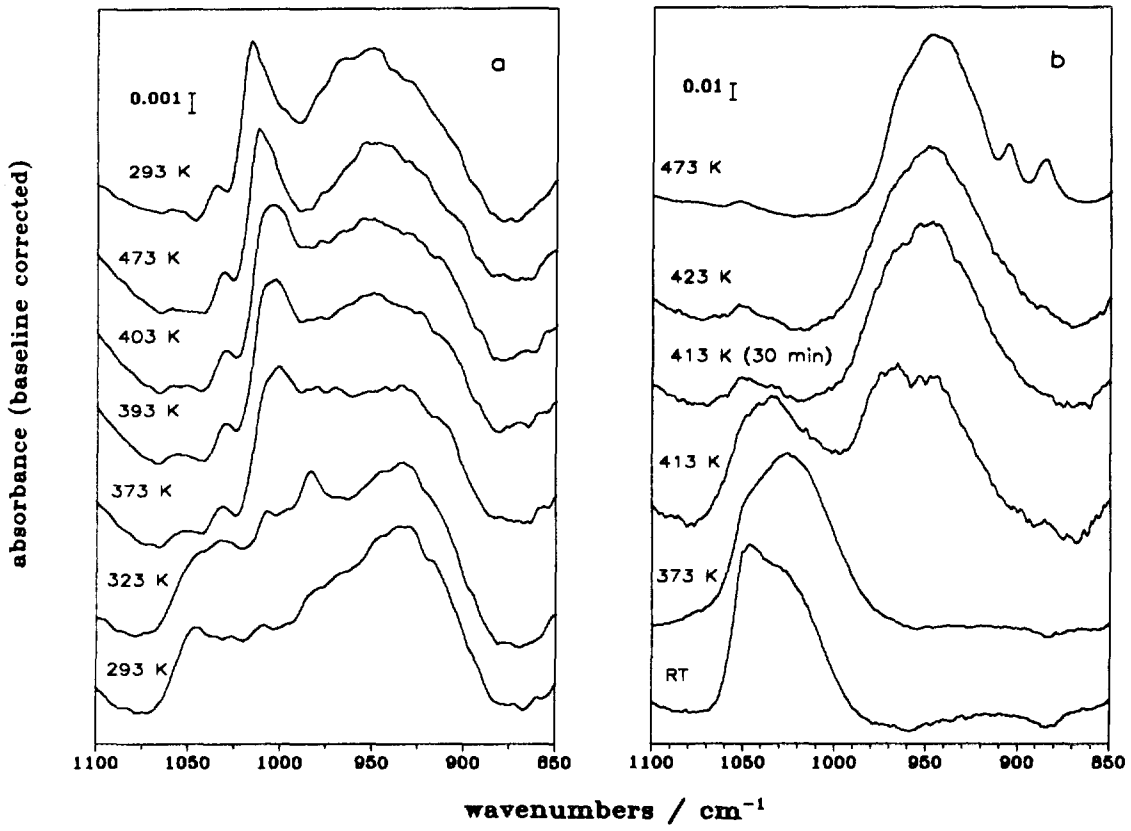

FIG. 4. *In situ* FTIR study of the calcination process. Spectra were recorded (bottom to top) as the temperature was raised to 473 K in steps of 50 K; 512 scans were recorded for each temperature. Two samples containing 3 wt% (a) and 30 wt% (b) of chromia were investigated. The top spectrum in (a) was recorded after cooling back to room temperature subsequent to calcination.

single pronounced maximum at 942 cm^{-1} had been observed (Fig. 4b).

Changes in OH stretching region occurring during calcination of the 30 wt% sample are monitored in Fig. 5. At 373 K, a broad and intense absorption due to associated water and hydroxyl groups extends up to 3750 cm^{-1}, such that titania hydroxyl absorptions are not detectable. During heating to 473 K, the water absorption decreases in intensity, and disappears completely after holding the sample at 473 K for 15 min. No hydroxyl vibrations that would be typical for either titania or chromia are observed.

The absence of specific chromium hydroxyl vibrations noted for the *in situ* calcined sample containing 30 wt% of CrO_x is confirmed by an FTIR investigation of the corresponding spectral region for samples with different chromia loadings (Fig. 6a). Pure titania (top trace) exhibits an intense composite band between 3600 and 3750 cm^{-1}; the latter is deconvoluted into four peaks at 3720, 3675, 3665, and 3646 cm^{-1}, which have been assigned to the anatase modification (38, 39).

A loading of 1 wt% of chromia on the surface (second trace) gives rise to a strong decrease in absorption of the ν(Ti–OH) vibrations, especially of the bands at 3720 and 3675 cm^{-1}. An additional broad band with a maximum at $\approx$3470 cm^{-1} appears in the spectrum, and is assigned to the O–H stretching vibration of chromium hydroxyl groups. Raising the coverage to 3 wt% of CrO_x again causes a drastic decrease of all hydroxyl vibrations, indicating a strong interaction of the supported chromia with the titania carrier. No Cr–OH absorptions are detectable for this loading. This trend is confirmed for the sample containing 10 wt% of CrO_x: no indications of ν(Cr–OH) bands are observed, and the titania hydroxyl vibrations have become very weak. The spectra recorded during *in situ* calcination are therefore in complete agreement with the results obtained for the *ex situ* calcined sample containing 30 wt% of CrO_x (Fig. 5, top trace).

After subsequent *in situ* reduction in hydrogen, the intensity of the hydroxyl vibrations is consistently higher (Fig. 6b). We note, in particular, the intense signal due to anatase OH groups in the sample containing 1 wt% chromia. Besides the broad maximum around 3470 cm^{-1} assigned to chromia hydroxyl groups, as mentioned above, another broad feature is observed around 3300 cm^{-1}. (On pure titania, bands at $\approx$3400 and $\approx$3300 cm^{-1}

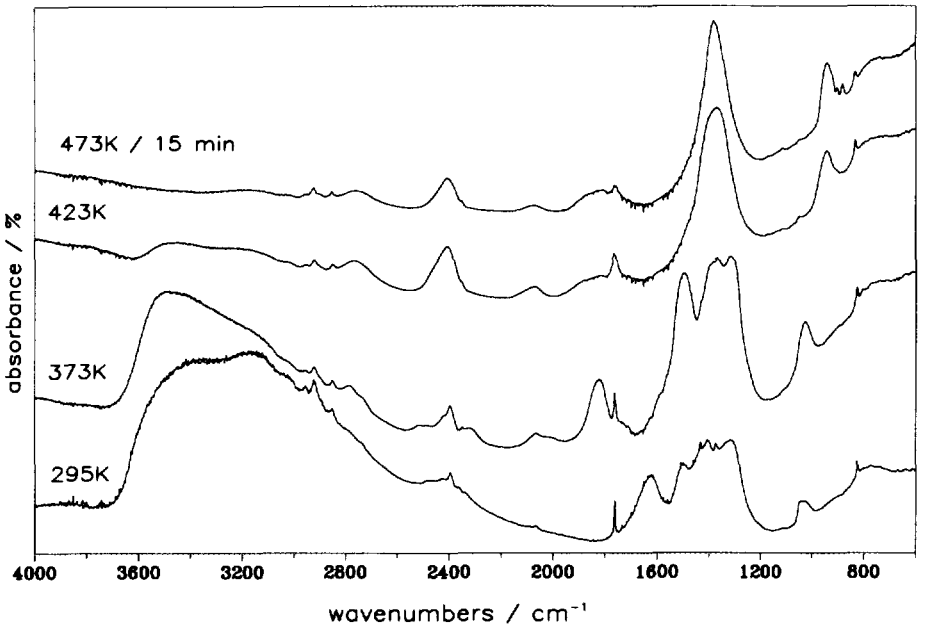

FIG. 5. *In situ* FTIR study of the calcination process for a 30 wt% CrO_x/TiO_2 sample. Wide range spectra are presented from which developments in the OH stretching region may be assessed. Experimental conditions are the same as in Fig

have been assigned to the rutile modification by Griffiths and Rochester (40). In our case, an attribution of the mentioned broad features to rutile appears unlikely as they are absent in the spectrum of the support, and are only observed with the chromia containing systems.) For a chromia loading of 3 wt%, the anatase-related signals appear drastically reduced in intensity, whereas the Cr–OH vibrations continue to be observed. At the highest chromia loading of 10 wt% displayed in Fig. 6b, only traces of these signals remain.

The results show that rehydroxylation of the surface CrO_x species by hydrogen only takes place for low chromia loadings. This observation may be related to the development of more compact double layers or multilayers, which are formed when the chromia loading exceeds the monolayer coverage. The multilayers appear to be comparatively inert towards hydrogen and, as a consequence, surface hydroxyl groups are only formed to a minor extent.

Significant changes are observed in this spectral region after samples have been exposed to SCR reaction conditions. Appearing bands are partly due to ammonia residing on the reduced surface. Spectroscopic investigations of CrO_x/TiO_2 catalysts exposed *in situ* to SCR conditions are in progress, and will be reported in another place.

Laser-Induced Changes on the Catalyst Samples

While the Raman spectra of Fig. 1 have been recorded at a low laser intensity of $\approx$5 mW cm^{-2}, which does not induce any alterations on the surface, time-dependent changes are observed when the intensity is raised to 12 mW cm^{-2}. These changes manifest themselves spectacularly to the observer in a time-dependent changing of the speckle pattern scattered from the sample. The spectra in Fig. 7 have been recorded on the multichannel detection system described in the experimental section. Rather than taking snapshots of the surface separated by periods of irradiation, we have chosen to accumulate the signal continuously on the multichannel detector *during* successive illumination periods of increasing length. This procedure offers the advantage of tremendously increasing the signal/noise ratio; yet the signal intensities remain comparable as they are normalized with respect to integration time.

A first, short detection period of 20 s leads to a unstructured spectrum (bottom trace in Fig. 7) with a very broad, weak band around 880 cm^{-1}. Of the titania vibrations, only the band at 636 cm^{-1} is clearly identified. After additional periods of signal integration, of increasing lengths as indicated in Fig. 7, a broad band at 880 cm^{-1}, with two shoulders at 922 and 806 cm^{-1}, is observed to develop. Three characteristic anatase vibrations at 640, 515, and 400 cm^{-1} are now clearly seen. Two additional bands at 546 and 391 cm^{-1} point to the existence of crystalline Cr_2O_3 particles on the surface. An integration time of 200 s leads to a sharpening of the band at 860 cm^{-1}; shoulders are observed at 980 and 772 cm^{-1}. In the range below 700 cm^{-1}, the anatase modes mentioned above develop into sharp peaks; minor bands at 546 and 431 cm^{-1} may be

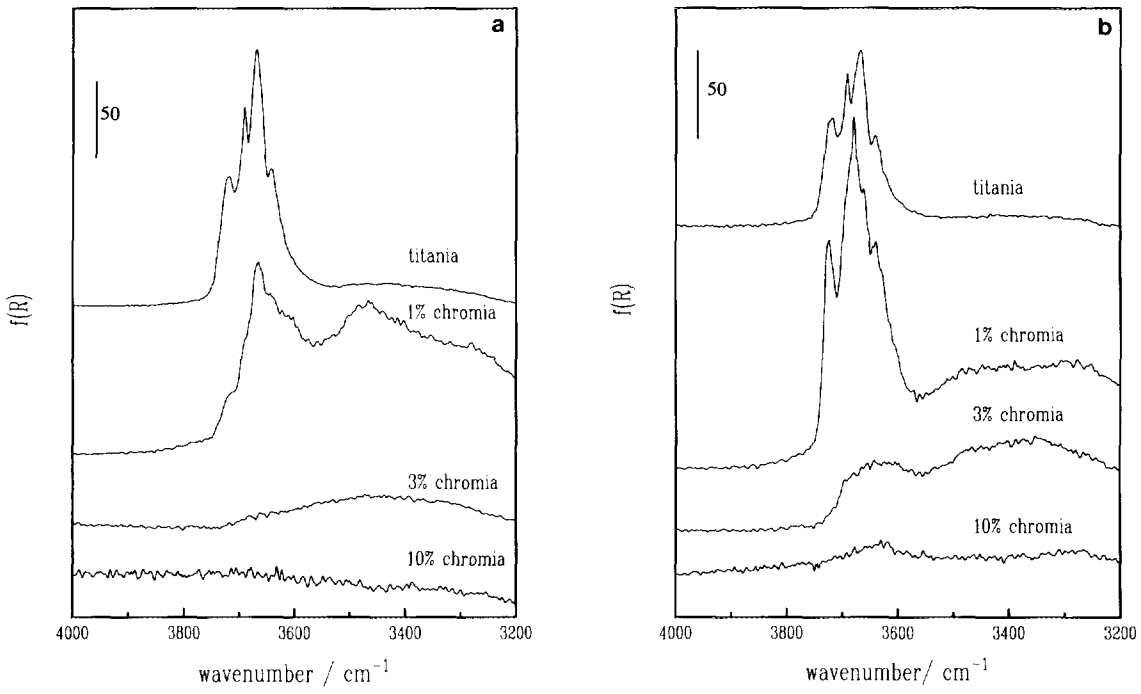

FIG. 6. Influence of the chromia content on the hydroxyl stretching vibrations. (a) DRIFT spectra (200 scans at a resolution of 4 cm^{-1}) were recorded at 298 K after samples were calcined *in situ* under a flow of 6% oxygen in argon at 573 K for 1 h. Spectra are presented for the pure titania support (top) and for catalyst samples containing 1, 3, and 10 wt% of chromia, as indicated in the figure. (b) Spectra recorded at 298 K after samples were exposed to a flow of 6% hydrogen in argon at 573 K for 1 h.

taken as hints to the formation of Cr_2O_3 and CrO_3. At higher integration times, the latter peaks become weaker, and have disappeared in the topmost spectrum.

At short observation times the intensity of the chromia-related bands exceeds that of the titania band; the noise level is high as a consequence of the (necessarily) short integration time and of the dark color of the sample. We note that the situation is completely changed after prolonged laser exposure. The titania bands now dominate in intensity; for the chromia vibrations around 800 cm^{-1}, a decrease in intensity and a loss of the (unresolved) fine structure are observed.

Laser-Induced Changes on the $Cr(NO_3)_3$ Precursor

In the bottom trace of Fig. 8, the Raman spectrum of the equally treated, but undiluted $Cr(NO_3)_3$ precursor is presented. A δ(Cr–O–Cr) deformational vibration at 217 cm^{-1} suggests the existence of polymeric oxochromium species. A broad, unstructured band is observed between 400 and 600 cm^{-1}, indicating an amorphous character of this reference sample. Laser exposure for 2000 s (second trace of Fig. 8) induces crystallisation yielding Cr_2O_3; the spectrum closely matches that of a commerical Cr_2O_3 sample (top trace).

The simultaneous presence of a minor fraction of Cr(VI) oxide in the laser-crystallised sample is indicated by a weak peak at 390 cm^{-1}; a reference spectrum of CrO_3 has been included in the third trace of Fig. 8 for comparison. We note that the higher frequency "doublet" in the laser-exposed sample, at 594 and 536 cm^{-1}, is down-shifted by $\approx$15 cm^{-1} with respect to the Cr_2O_3 reference spectrum; this shift is attributed to a support influence.

Influence of Calcination Temperature

In view of the pronounced changes observed during laser irradiation, it was deemed important to assess the influence of duration and temperature of the calcination treatment employed in the catalyst preparation. In particular, we investigate whether there are threshold temperatures for the development of structural elements on the surface.

The results, presented in Fig. 9, parallel the trends observed during laser irradiation. After 1.5 h of calcination at 473 K, a dominating broad band at 870 cm^{-1} with a shoulder around 900 cm^{-1} is observed. In the range below 700 cm^{-1}, anatase vibrations are detected; bands at 546 and 606 cm^{-1} are assigned to Cr_2O_3 particles. Further changes occur if the calcination time at 473 K is extended to 3 h (right diagram); the bands appear to sharpen, as surface heterogeneity and hence the inhomogeneous broadening are reduced.

A very similar spectrum is recorded already after

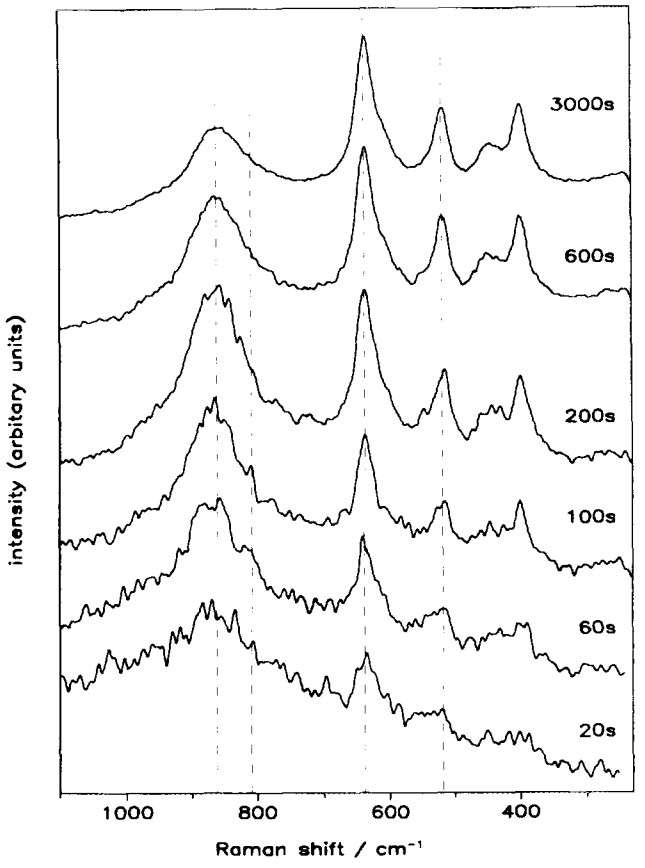

FIG. 7. Changes in chromia surface species induced by laser irradiation (12 mW cm^{-2}) observed with an *ex situ*-calcined 10 wt% CrO_x/TiO_2 sample. The state of the surface is monitored with a multichannel detection system (cf. Experimental section) during subsequent laser exposures, for the incremental times indicated in the figure.

1.5 h of calcination at the higher temperature of 573 K. Titania and chromia peaks are of comparable intensities; observation of the δ(Cr–O–Cr) vibration at 203 cm^{-1} indicates the presence of extended chromia clusters (tetrameric species according to Ref. (1)) on the surface of the P25 support. After 3 h of calcination at 573 K, pronounced changes in intensities are noted: the relative strength of the titania vibrations is increasing, and a broad shoulder around 750 cm^{-1} develops on the low-frequency side of the band at 860 cm^{-1}.

When a calcination temperature of 673 K is used, changes appear to be complete already after 1.5 h; the spectrum recorded after 3 h is very similar. Broad residual bands are observed at 840 and 960 cm^{-1}. Titania vibrations, due to both anatase and rutile (430 cm^{-1}), have strongly increased in intensity.

DISCUSSION

Several trends are identified as a function of the chromia loading on the titania support, for the chosen impregnation/calcination procedure. At the lowest coverage of 0.5 wt% CrO_x, isolated tetrahedral chromate species are prevailing, which are distorted by interaction with the support surface (1, 22, 23). Agglomeration of the chromia surface species starts at a loading of 3 wt%; this is concluded from the appearance of Raman bands due to larger clusters. The formation of trimeric and tetrameric species is indicated by the observation of vibrations at 840, 942, and 907 cm^{-1}, which are identified from the deconvolution of the broad band around 860 cm^{-1}.

While the observation of isolated chromate species for low coverages is in agreement with the results of Hardcastle and Wachs (1), these authors did not report trimeric species on the 3 wt% catalyst described in Ref. (1). The difference may be due to the different calcination procedures used, and to the handling of our catalysts under ambient conditions.

The coexistence of several oxidation states on the surface subsequent to calcination is noteworthy, and may be attributed to the comparably mild conditions applied.

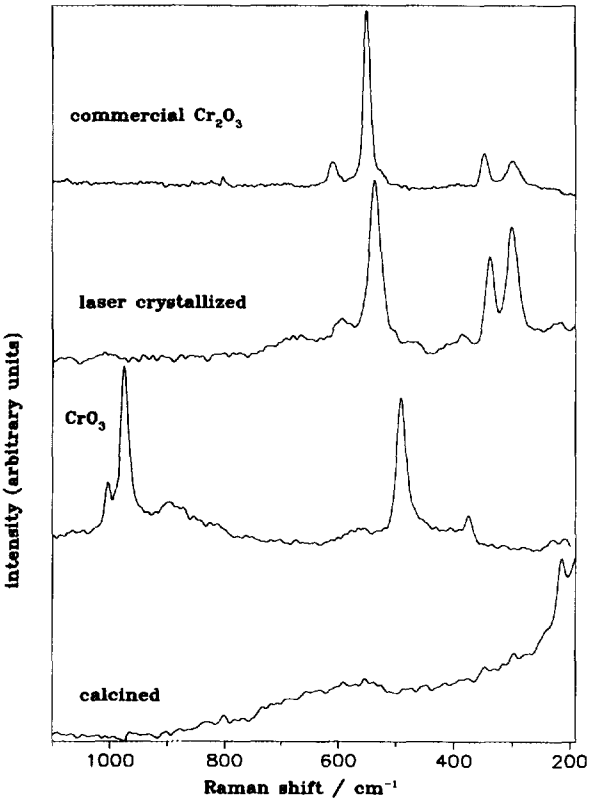

FIG. 8. Laser induced crystallisation of the unsupported similarly treated $Cr(NO_3)_3$ precursor. Bottom to top: (a) spectrum recorded subsequent to *ex situ* calcination using a low laser intensity (6 mW cm^{-2}) and an integration time of 1800 s; (b) reference spectrum of commercial CrO_3; (c) spectrum of sample after exposure to high laser intensity (12 mW cm^{-2}) during an integration time of 2000 s; (d) reference spectrum of commercial α-Cr_2O_3.

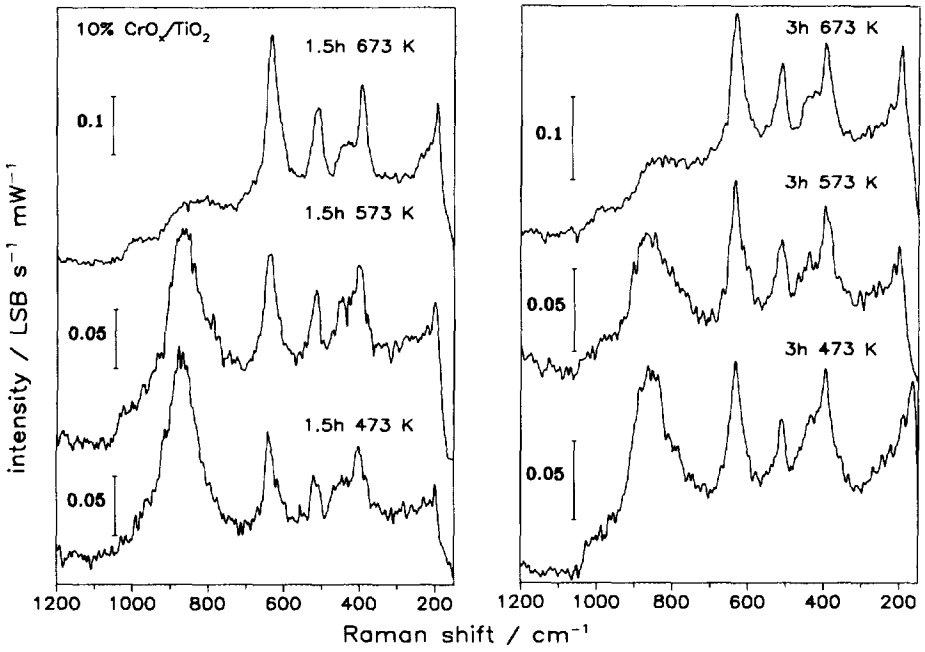

FIG. 9. Influence of duration and temperature of *ex situ* calcination for a sample containing 10 wt% of chromia on titania. Low power Raman spectra are compared for samples that had been calcined for 1.5 h (left diagram) and for 3 h (right diagram), at the temperatures indicated in the figure.

Similar mixed valence states have been reported by Cimino *et al.* (5b) for a CrO_x/ZrO_2 catalyst calcined and evacuated at different temperatures, and by Jagannathan *et al.* (9) for CrO_x/Al_2O_3 catalysts with higher chromia contents, which had been subjected to mild reduction after calcination.

The oxidation states VI, V, and III of chromium have been identified on all of our calcined catalyst samples. With increasing chromia loading, the fraction of Cr(V) decreases, whereas that of Cr(III) is observed to increase. In the escape depth probed by XPS, the surface layer of the *uncalcined* 30 wt% chromia/TiO_2 catalyst exhibits only Cr(V) signals. This prevalence is due to oxidation of the outermost surface layers by atmospheric oxygen, or by the NO_3^- ion, which is simultaneously reduced to NO_x (7). These oxidation processes give rise to coordinatively unsaturated surface chromium ions, with a formal oxidation state near V.

When comparing the results of the present study with those of our earlier EPR investigation (7), one has to take into account the different sampling depths. While the EPR signal comprises all spins present in the sample, the outermost few layers are preferentially detected by XPS; the same applies to UV–visible diffuse reflectance spectroscopy of the more strongly colored samples. The existence of ferromagnetic CrO_2 (oxidation state +4) on the highly concentrated calcined catalysts has been proposed from the EPR results (7). We have obtained some evidence for the presence of CrO_2 from diffuse reflectance spectra, and have found that the binding energy of the component referred to as "Cr(III)" throughout the text is compatible with the involvement of Cr(IV) as well.

With regard to the other oxidation states, there is general agreement between the results obtained from the three spectroscopic techniques, from temperature programmed reduction, and from thermoanalytic measurements (8). Smaller differences mentioned above are well explained by taking into account the specific information probed by the various methods. Concordant results of all the mentioned techniques are the simultaneous existence of the oxidation states +3, +5, and +6, structural features such as the formation of polynuclear Cr(III) species, and the development of crystalline Cr_2O_3 on the surface which depends on the chromia content. In addition, the survey on all observations shows a depth dependence of the oxidation state within the chromia agglomerates. A kernel of Cr(III) is covered by outer layers consisting mainly of Cr(V) and Cr(VI); interaction between Cr(III) and the species in higher oxidation states is seen in the calcined catalysts.

According to the distinct antiferromagnetic coupling of the Cr(V) species to other chromium surface species found by EPR (7), the differences in the Cr(V) amounts observed by EPR on the one hand, and by XPS and diffuse reflectance on the other hand, had to be expected. Strongly antiferromagnetically coupled Cr(V) species are EPR silent. Correspondingly, no Cr(V) EPR signal was observed for chromia contents <5 wt%, whereas the

Cr(V) portions found by XPS and diffuse reflectance are remarkable. Differences in the relative contents of other oxidation states of chromium can be explained in the same manner. The XPS-derived presence of Cr(VI) is quite expected for the outermost layers of the oxidized samples. The hydrogen consumption values of the TPR experiments (8) are in good qualitative agreement with the XPS results.

The *in situ* calcination studies show interesting parallels to the EPR investigations (7), where the Cr^{3+} concentration was found to decrease in favour of appearing Cr(V) and Cr(VI) species. Corresponding FTIR studies have been performed for catalysts containing 3, 16 (not shown in Fig. 4), and 30 wt% of chromia, respecively. In all the *in situ* studies performed on small quantities of powdered sample, the surface oxidation reaction was found to take place at temperatures below 423 K. Under the comparatively mild oxidation conditions used in the cell (slow heating to 473 K), Cr^{3+} is oxidized to coordinatively unsaturated chromyl species for the lowest loading (3 wt%). These species differ in the types of bridging surface ligands, and correspond to oxidation states close to V. With the higher chromia loadings of 16 and 30 wt%, Cr^{3+} was found to be oxidized up to an oxidation state near VI, whereby coordinatively saturated surface chromyl groups with a Cr=O bond order near two are formed.

The results obtained on catalysts subjected to *ex situ* calcination show some mass transport effects. For the somewhat larger quantity (10 g) of uncrushed catalyst cake, a time of 3 h is required at 473 K to complete the oxidation process; at the higher temperature of 673 K oxidation is complete after 1.5 h. From the Raman spectra, the resulting chromia surface species are found to depend on the calcination conditions. Chromia-related bands decrease during longer calcination and/or at higher temperature. The most striking change in Fig. 9 is the decrease of the chromia vibrations between 800 and 900 cm^{-1}, as opposed to a strong intensity increase of the anatase vibrations below 650 cm^{-1}. A similar decrease for 1 and 3 wt% of chromia on TiO_2 has been reported by Hardcastle and Wachs (1) for calcination at 773 and 973 K. In the light of the EPR results (7), our observation can be interpreted in terms of a solid state reaction in which the chromium ions are incorporated in the lattice of the support oxides.

We did not observe the formation of a lower oxidation state species as a product of laser-induced reduction as suggested by Hardcastle and Wachs (1), and no shift of the Raman bands to higher wavenumbers was found to take place. Such a shift had been described for chromia on SiO_2 by Kim *et al.* (41), and was attributed to a decomposition of larger clusters, and a stronger interaction with the silica support.

The effect of laser exposure on the supported samples (Fig. 7) is similar to that of calcination. Strong titania bands appear, whereas the chromia-related vibrations are observed to decrease. Yet, even after a total exposure time of 4000 s, the Raman doublets that are typical of Cr_2O_3 (609/551 cm^{-1} and 348/298 cm^{-1}, cf. top trace of Fig. 8) did not appear in the spectra. In contrast, the pure $Cr(NO_3)_3$ reference sample subject to the same sequence of preparation steps was observed to change from amorphous CrO_x into crystalline Cr_2O_3. Thus, the interaction of the chromia with the titania support appears to prevent the crystallization. The observation of a growth in intensity of anatase vibrations during both calcination and laser exposure demonstrates that a larger fraction of the titania surface becomes uncovered. Therefore we conclude, in accordance with EPR, that a solid state reaction between chromia and titania involving migration of chromium ions into the titania support oxide (mainly, into the rutile lattice) is taking place.

CONCLUSIONS

Several trends have been identified as a function of the chromia loading on the surface of titania (P25). With increasing coverage, the prevalent surface species are observed to change from isolated, tetrahedrally coordinated species to agglomerated larger clusters, with spectral characteristics resembling those of tri- and tetrameric chromates.

On the surface of the supported chromia catalysts, at least three oxidation states (Cr(III), Cr(V), and Cr(VI)) coexist. The relative contributions of the three oxidation states change with the loading, with the calcination treatment, and with storage under atmospheric conditions. At low coverages Cr(V) species dominate, whereas for a chromia content of 30 wt%, approximately equal fractions of the three states have been found by XPS.

In situ studies show that the Cr^{3+} ions of the precursor are oxidized to coordinatively unsaturated chromyl surface species with an oxidation state near V at lower coverages. At higher coverages, calcination results in coordinatively saturated chromia centers anchored on the titania support (formal oxidation state near VI in the terminology of Ref. (15)).

The resulting chromia species are observed to depend on the calcination conditions. Under an oxygen atmosphere, transformation appeared to be complete after 3 h at 473 K, or alternatively after 1.5 h at 673 K. Longer calcination times or higher calcination temperatures give rise to a decrease of the chromia-related bands, and an increase in intensity of the support vibrations in the Raman spectrum. This effect is also observed to take place under intense laser irradiation. By comparison, the similarly treated $Cr(NO_3)_3$ precursor merely undergoes crystallisation under the same conditions. We infer that a solid

state reaction involving incorporation of chromia into the titania support, as addressed in Part I [7], is occurring at higher temperatures.

ACKNOWLEDGMENTS

We are thankful to G. Sauer for recording the XPS spectra, and to W. Häfner for providing the software for spectral deconvolution. Financial support of this work by the Deutsche Forschungsgemeinschaft (SFB 213) and by the Schweizerische Nationalfonds (NFP 24) is gratefully acknowledged.

REFERENCES

1. Hardcastle, F. D., and Wachs, I. E., *J. Mol. Catal.* **46,** 173 (1989).
2. Vuurman, M. A., Stufkens, D. J., Oskam, A., Moulijnardt, J. A., and Kapteijn, F., *J. Mol. Catal.* **60,** 83 (1990).
3. Biffar, W., Drews, R., Hess, K., Lehnert, R, Mross, W. D., and Scheidsteger, O., *Brennsl. Waerme Kraft* **38,** 211 (1986).
4. Curry-Hyde, E., and Baiker, A., *Ind. Eng. Chem. Res.* **29,** 1985 (1990); Curry-Hyde, H. E., Musch, H., and Baiker, A., *Appl. Catal.* **65,** 211 (1990); and Curry-Hyde, H. E., Musch, H., Baiker, A., Schraml-Marth, M., and Wokaun, A., *J. Catal.* **133,** 397 (1992).
5. (a) Cimino, A., De Angelis, B. A., Luchetti, A., and Minelli, G., *J. Catal.* **45,** 316 (1976);
(b) Cimino, A., Cordischi, D., Febbraro, S., Gazzoli, D., Boccuzzi, F., Chiorino, A., and Ghiotti, G., *J. Mol. Catal.* **55,** 23 (1989), and Refs. 24–27 cited therein.
6. Zecchina, A., Coluccia, S., Guglielminotti, E., and Ghiotti, G., *J. Phys. Chem.* **75,** 2774 (1971).
7. Köhler, K., Schläpfer, C. W., von Zelewsky, A., Nickl, J., Engweiler, J., and Baiker, A., *J. Catal.* **143,** 201 (1993). [Part I of this study].
8. Engweiler, J., Nickl, J., Baiker, A., Köhler, K., Schläpfer, C. W., and von Zelewsky, A., *J. Catal.* **145,** 000 (1994). [Part II of this study].
9. Jagannathan, K., Srinivasan, A., and Rao, C. N. R., *J. Catal.* **69,** 418 (1981).
10. McDaniel, P., *J. Catal.* **76,** 17 (1982).
11. Cimino, A., Cordischi, D., De Rossi, S., Ferraris, G., Gazzoli, D., Indovina, V., Minell, G., Occhiuzzi, M., and Valigi, M., *J. Catal.* **127,** 744 (1991).
12. Stein, P., Miskowski, V., Woodruff, W. H., Griffin, J. P., Werner, K. G., Gaber, B. P., and Spiro, T. G., *J. Chem. Phys.* **64,** 2159 (1976).
13. Miyamoto, A., Ut, T., and Murakami, Y., *J. Catal.* **80,** 106 (1983).
14. Carrott P. J. M., and Sheppard, N., *J. Chem. Soc. Faraday Trans.* **79,** 2425 (1983).
15. Schraml-Marth, M., Wokaun, A., Curry-Hyde, H. E., and Baiker, A., *J. Catal.* **133,** 415 (1992), and references cited therein.
16. Indovina, V., Cordischi, D., De Rossi, S., Ferraris, G., Ghiotti, G., and Chiorino, A., *J. Mol. Catal.* **68,** 53 (1991).
17. Grünert, W., Shipiro, E. S., Feldhaus, R., Anders, K., Antoshin, G. V., and Minachev, Kh. M., *J. Catal.* **100,** 138 (1986).
18. Meier, M., Carron, K. T., Fluhr, W., and Wokaun, A., *Appl. Spectrosc.* **42,** 1066 (1988).
19. Schild, Ch., Wokaun, A., and Baiker, A., *Surf. Sci.* **269/270,** 520 (1992).
20. Beattie, L. R., and Gilson, T. R., *J. Chem. Soc.*, 2322 (1969).
21. Porto, S. P. S., Fleury, P. A., and Damen, T. C., *Phys. Rev.* **154,** 522 (1967).
22. Michel, G., and Cahay, R., *J. Raman Spectrosc.* **17,** 4 (1986).
23. Michel, G., and Machiroux, R., *J. Raman Spectrosc.* **14,** 22 (1983).
24. Zecchina, A., Garrone, E., Ghiotti, G., Morterra, C., and Borello, E., *J. Phys. Chem.* **79,** 966 (1975).
25. Bailey, N., Carrington, A., Lott, K. A. K., and Symons, M. C. R., *J. Chem. Soc.*, 290 (1960).
26. Louis, C., and Che, M., *J. Catal.* **135,** 156 (1992).
27. Scharf, U., Schraml-Marth, M., Wokaun, A., and Baiker, A., *J. Chem. Soc. Faraday Trans. I* **87,** 3299 (1991).
28. Sutton, D., *in* "UV Atlas of Organic Compounds," Vol. 5, spectrum K1/20. Verlag Chemie, Weinheim, 1971.
29. Krauss, H. L., private communication.
30. Best, S. A., Squires, R. G., and Walton, R. A., *J. Catal.* **47,** 292 (1977).
31. Cimino, A., De Angelis, B. A., Luchetti, A., and Minelli, G., *J. Catal.* **45,** 316 (1976).
32. Allen, G. C. and Tucker P. M., *Inorg. Chim. Acta* **16,** 41 (1976).
33. Okamoto, Y., Fujii, M., Imakana, T., and Teranishi, S., *Bull. Chem. Soc. Jpn.* **49,** 859 (1976).
34. Wagner, C. D., Riggs, W. M., Davis, L. E., Moulder, J. F., and Mullenberg, G. E., "Handbook of X-Ray Photoelectron Spectroscopy." Perkin–Elmer Corporation, 1979.
35. Seifert, H., "Anwendungen der Schwingungsspektroskopie in der anorganischen Chemie." Springer, Berlin, 1966.
36. Marshall, R., Mitra, S. S., Gielisse, P. J., Plende, J. N., and Mansur, L. C., *J. Chem. Phys.* **43,** 2893 (1965).
37. Mattes, R., *Z. Anorg. Allg. Chem.* **311,** 102 (1961).
38. Topsøe, N-Y. *J. Catal.* **128,** 499 (1991).
39. Busca, G., Saussey, H., Saur, O., Lavalley, J. C., and Lorenzelli, V., *Appl. Catal.* **14,** 245 (1985).
40. Griffiths, D. M., and Rochester, C. H., *J. Chem. Soc. Faraday Trans. I* **73,** 1510 (1977).
41. Kim, Du Soung, Tatibouet, J.-M., and Wachs, I. E., *J. Catal.* **136,** 209 (1992).